Proceedings of the ASME 2015 34th International Conference on Ocean, Offshore and Arctic Engineering
OMAE2015
May 31-June 5, 2015, St. John's, Newfoundland, Canada

OMAE2015-41691

COMPARISON OF *AQWA*, *GL RANKINE*, *MOSES*, *OCTOPUS*, *PDSTRIP* AND *WAMIT* WITH MODEL TEST RESULTS FOR CARGO SHIP WAVE-INDUCED MOTIONS IN SHALLOW WATER

Tim Gourlay
Centre for Marine Science and Technology, Curtin University
Perth, Australia

Alexander von Graefe
DNV GL
Hamburg, Germany

Vladimir Shigunov
DNV GL
Hamburg, Germany

Evert Lataire
Maritime Technology Division, Ghent University
Ghent, Belgium

ABSTRACT

A benchmarking study is carried out concerning wave-induced ship motions in shallow water, predicted with commercially available codes *AQWA*, *GL Rankine*, *MOSES*, *OCTOPUS*, *PDStrip* and *WAMIT*. Comparison is made with experiments for three cargo ship models tested at Flanders Hydraulics Research. The same IGES models of the ship hulls were used in all codes to ensure consistent representation of the model geometry. The comparisons may be used to assess the suitability of each code for zero-speed applications such as berthed ship motions and under-keel clearance, as well as forward-speed applications such as under-keel clearance in navigation channels. Another, quickly developing, application area that requires analysis of seaway-induced ship motions in shallow water, is analysis of motions, accelerations and loads on cargo transport, installation and service vessels for offshore wind parks.

INTRODUCTION

Table 1 shows software used for this benchmarking study. Three ships were considered, under conditions for which published model test data are available. The model tests were undertaken at Flanders Hydraulics Research and are described in *Vantorre and Journée (2003)* and *Vantorre et al. (2008)*. The test cases are:

- Ship F (panamax container ship) at water depth 13.6 m, concerning heave, pitch and roll in head waves at 0, 8 and 12 knots forward speed and in beam waves at zero speed;
- Ship G (panamax bulk carrier) at water depth 13.6 m, concerning heave, pitch and roll in head waves at 8 and 10 knots and in beam waves at zero speed;
- Ship D (post-panamax container ship) at water depth 18.0 m, concerning heave, pitch and roll in head waves at 12 knots and waves 10° off-stern at 12 knots.

Heave refers here to the centre of gravity. Principal particulars of the test ships are shown in Table 2 in full scale. Table 3 provides coordinate systems used.

GEOMETRY PREPARATION

For all test ships, geometry was provided as an IGES model by Ghent University and Flanders Hydraulics Research.

Software *MAXSURF* was used to generate a regular grid of offset points for *OCTOPUS*, using equally-spaced stations between the aft and forward submerged extremities and equally-spaced waterlines from the keel to the calm waterline. Where the hull does not extend across all waterlines, offsets are modified to ensure even number of intervals for each waterline spacing, *Journée (2001)*. The same offsets were used for *PDStrip* as for *OCTOPUS*, apart from replacing zero-area sections at the forward and aft extremities with small positive-area sections for *PDStrip* setup.

The 3D mesher of *OCTOPUS* was used to generate a surface mesh both for *WAMIT* and *MOSES*, resulting in a combined quadrilateral and triangular mesh. In addition, *MOSES* automatically splits panels that exceed pre-defined curvature criteria.

GL Rankine uses hull geometry description in STL format, and automatically generates unstructured triangular panel grid on the ship hull and block-structured quadrilateral grid on the free surface. The unstructured triangular grid on the ship hull is the same in the nonlinear steady solution and in the linear seakeeping solution, whereas free-surface grids differ between the nonlinear steady solver and the linear seakeeping solver.

The grids on the free surface used in the steady solution are automatically adjusted to ship dimensions, ship speed and water depth, whereas the grids on the free surface used in seakeeping solutions are automatically adjusted to ship speed and wave frequency and direction.

Table 1: Software used for benchmarking study

Program, Version	Type	Forward Speed	Shallow Water	Developer	Reference	Calculations done by
AQWA 14.5	Radiation/diffraction panel code	no	Shallow-water Green functions	ANSYS	*Ansys Inc. (2010)*	DNV GL
GL Rankine Rel. 2.0	Rankine-source patch code	yes	Symmetry condition or panels	DNV GL	*Söding et al. (2012), von Graefe (2014)*	DNV GL
MOSES 7.06	Radiation/diffraction panel code	no	Shallow-water Green functions	Bentley Systems	*Ultramarine (2012)*	CMST
OCTOPUS 6.3.0	Strip theory code	yes	*Keil (1974)* shallow-water hydrodynamic coefficients	Amarcon	*Amarcon (2009)*	CMST
PDStrip rev. 27	Rankine-source strip theory code	yes	Symmetry condition	H. Söding	*Söding (2006)*	CMST
WAMIT 7.062	Radiation/diffraction panel code	no	Shallow-water Green functions	WAMIT Inc.	*WAMIT (2013)*	CMST

Table 2: Principal particulars of ships

	L_{pp} [m]	B_{wl} [m]	T [m]
Ship F	190.00	32.00	11.60
Ship G	180.00	33.00	11.60
Ship D	291.13	40.25	15.00

Table 3: Coordinate system used by ship motion programs

Program	Coordinate origin	*x*-axis	*y*-axis	*z*-axis
OCTOPUS	keel, AP	forward	to port	upward
PDStrip	keel, L_{CG}	forward	to port	upward
WAMIT	waterline, L_{CG}	forward	to port	upward
AQWA	waterline, L_{CG}	forward	to port	upward
GL Rankine	waterline, L_{CG}	forward	to port	upward
MOSES	keel, front of bulb	aft	to starboard	upward

For better comparison, the panel grids on the ship hulls generated with *GL Rankine* were used also for *AQWA*.

For all codes, ship motion results were found to be robust with respect to discretization of the ship hull, and grid fineness was generally much larger than required.

SOLVER SETTINGS

In *OCTOPUS*, radiation and diffraction problems were solved using approach described in *Journée and Adegeest (2003)*, p. 219. The "modified strip theory" method was used, *Journée and Adegeest (2003)*, p. 197. The shallow-water hydrodynamic coefficients were computed using method of *Keil (1974)*.

PDStrip uses a strip-wise Rankine source method, with a symmetry condition on the seabed to model shallow water. No flow separation was specified along the hull, linear seakeeping method was used, and transom was set up as wet at zero forward speed and dry at non-zero forward speeds.

In *WAMIT*, all calculations were done using the low-order method, *WAMIT (2013)*, p. 6-1. The iterative solver *WAMIT (2013)*, p. 14-4, was used where possible, however for Ship G at low frequencies, this solver failed to converge, and therefore the direct solver *WAMIT (2013)*, p. 14-4, was used. In *MOSES*, all calculations were done using a 3D diffraction solver, *Ultramarine (2012)*, p. 257.

GL Rankine uses three different seakeeping solvers: Rankine source-patch method with linearisation around nonlinear steady flow, Rankine source-patch method with linearisation around double-body steady flow (used for the present test cases due to the relatively low forward speeds) and zero-speed free-surface Green function method with encounter frequency correction for forward speed effects. Bottom was modelled using symmetry condition in both steady and seakeeping solutions.

In *AQWA*, shallow-water zero-speed free-surface Green functions were used to take into account shallow-water effects.

Roll damping was applied as follows: in *OCTOPUS*, the Ikeda method was used, which is an empirical method including viscous effects, *Journée and Adegeest (2003)*, p. 184; in *PDStrip* and *WAMIT*, the default method was used, which includes only potential damping; in *MOSES*, the default Tanaka method was used, *Ultramarine (2012)*, p. 251, which is a semi-empirical method including viscous effects; in *GL Rankine*, roll damping was set to 10% (Ship F and Ship G) and 5% (Ship D) of critical damping. It is recognized that because of the importance of viscous effects on roll damping, and the varying treatment of these by the different software packages, roll amplitudes cannot be directly compared. The authors have made deliberately no attempt to match the roll damping characteristics in the used software packages, because such an attempt would have been largely a curve-fitting exercise.

Computations with *WAMIT* and *GL Rankine* were done with two different setups: first, the ship was considered free in heave, pitch and roll but fixed at the centre of gravity in surge, sway and yaw, following the setup used in the model tests, and, second, the ship was set free in all degrees of freedom (which is the only option possible in *OCTOPUS*, *PDStrip* and *MOSES*) to provide results for comparison with the other numerical methods.

SHIP F: PANAMAX CONTAINER SHIP

The body plan and principal particulars of this hull, together with model test conditions, are given in *Vantorre and Journée (2003)*. Roll radius of inertia of 11.7 m (36.6% of B_{wl}) was used for *MOSES*, *OCTOPUS*, *PDStrip* and *WAMIT*, and 12.1 m (37.8% of B_{wl}) in *GL Rankine* and *AQWA*.

OCTOPUS used 49 sections in the longitudinal direction and 21 offset points along each section; the resulting sections are shown in Figure 1. The same model was used in *PDStrip*.

The *WAMIT* grid was generated using 80 panels in the longitudinal direction and 25 panels along each section for the main part of the hull, and 8 and 20 panels, respectively, to model the bulb. The hull was meshed up to the calm waterline. This resulted in a combined quadrilateral and triangular mesh with 2160 panels on the port side, Figure 2.

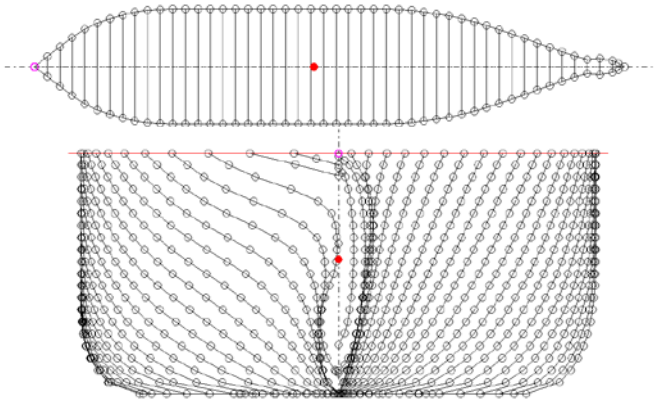

Figure 1: Sectional offsets for Ship F used in *OCTOPUS* and *PDStrip*

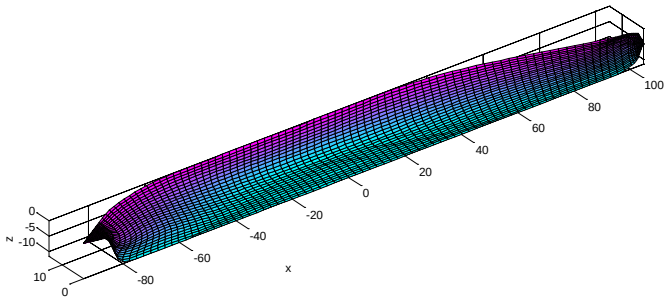

Figure 2: Panel mesh for Ship F used in *WAMIT*

The *MOSES* panel grid used 50 panels in the longitudinal direction and 15 panels along sections for the main hull and 5 and 12 panels, respectively, for the bulb. Hull was meshed up to the calm waterline. This resulted in a combined quadrilateral and triangular mesh with 1620 panels on the whole hull, Figure 3 (top). *MOSES* automatically splits panels which exceed pre-defined curvature limit; Figure 3 (bottom) shows the final mesh used by *MOSES*.

Figure 4 shows a grid on the half ship (1433 panels), automatically generated by *GL Rankine*, which was used in *GL Rankine* and *AQWA* computations.

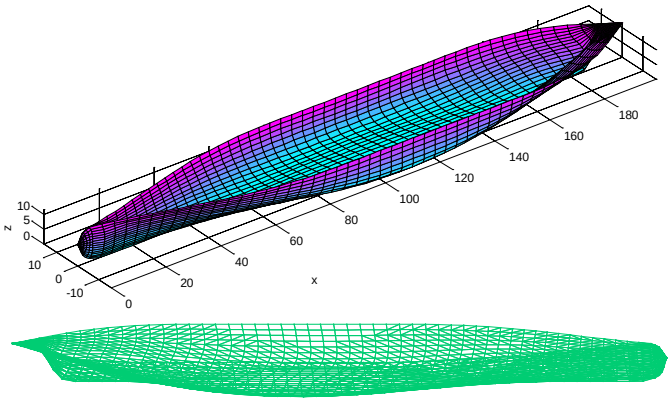

Figure 3: 1620-panel whole-hull mesh for Ship F read into *MOSES* (top) and final 2818-panel mesh used in *MOSES* (bottom)

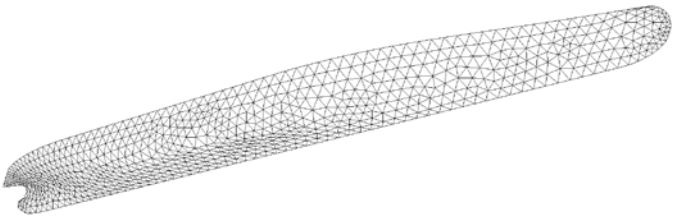

Figure 4: Panel mesh for Ship F used in *GL Rankine* and *AQWA* computations

SHIP G: PANAMAX BULK CARRIER

The body plan and principal particulars of this hull, together with model test conditions, are given in *Vantorre and Journée (2003)*. Roll radius of inertia of 14.8 m (44.8% of B_{wl}) was used in *MOSES*, *OCTOPUS*, *PDStrip* and *WAMIT*, and 15.2 m (46.0% of B_{wl}) in *GL Rankine* and *AQWA*.

OCTOPUS used 49 sections in the longitudinal direction and 21 offset points along each section; the resulting sections are shown in Figure 5. The same hull discretization was used in *PDStrip*.

The *WAMIT* grid was generated using 80 panels in the longitudinal direction and 25 panels along each section for the main part of the hull, 8 and 20 panels, respectively, to model the bulb and 4 and 8 panels, respectively, to model transom. The hull was meshed up to the calm waterline. This resulted in a combined quadrilateral and triangular mesh with 2192 panels on the port side, Figure 6.

The *MOSES* panel grid used 50 panels in the longitudinal direction and 15 panels along sections for the main hull, 6 and 15 panels, respectively, for the bulb and 4 and 8 panels, respectively, for transom. Hull was meshed up to the calm waterline. This resulted in a combined quadrilateral and triangular mesh with 1744 panels on the whole hull, Figure 7 (top). *MOSES* automatically split panels that exceed pre-defined curvature limit; Figure 7 (bottom) shows the final mesh used by *MOSES*.

Figure 8 shows a grid on the half ship (1126 panels), automatically generated by *GL Rankine*, which was used in *GL Rankine* and *AQWA* computations.

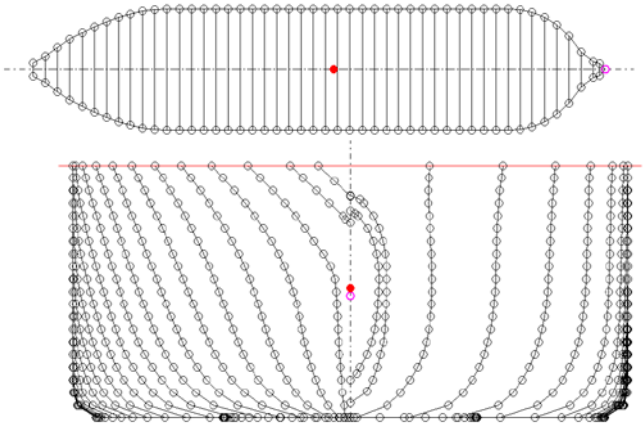

Figure 5: Sectional offsets for Ship G used in *OCTOPUS* and *PDStrip*

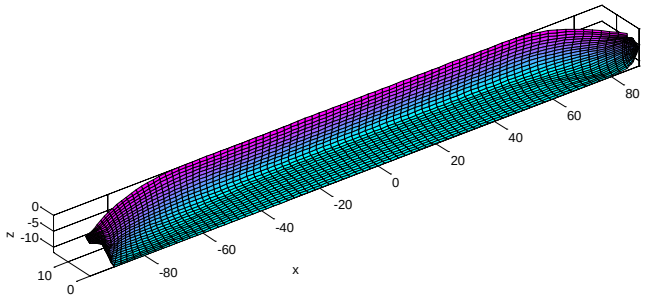

Figure 6: 2192-panel port-side mesh for Ship G used in *WAMIT*

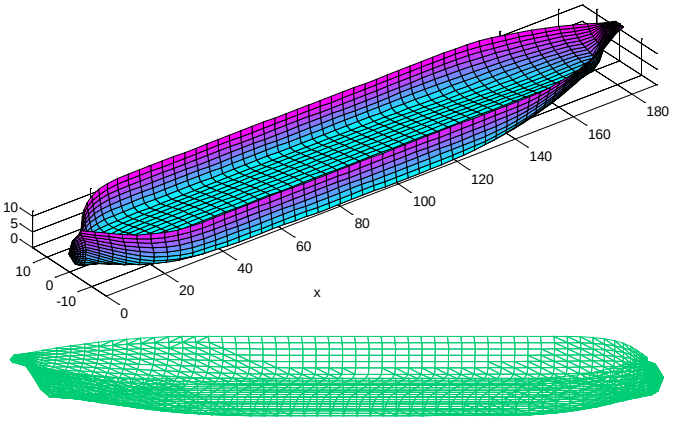

Figure 7: 1744-panel whole-hull mesh for Ship G read into *MOSES* (top) and final 2530-panel mesh used for computations in *MOSES* (bottom)

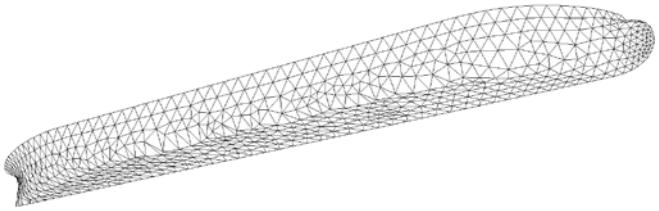

Figure 8: Panel mesh for Ship G used in *GL Rankine* and *AQWA* computations

SHIP D: 6000 TEU CONTAINER SHIP

The body plan is given in *Vantorre et al. (2002)*; principal particulars and model test conditions are given in *Vantorre et al. (2008)*. Roll radius of inertia of 33.0% of B_{wl} and pitch radius of inertia of 25% of L_{pp} were used in the model tests and calculations. Because tests were done at a full-scale speed of 12 knots, no calculations were done with *AQWA*, *MOSES* and *WAMIT*.

OCTOPUS used 49 sections in the longitudinal direction and 21 offset points along each section. To ensure proper meshing of the hull, the bulbous and flared section at 289.369 m from AP was given a small non-zero half-breadth above the bulb. The resulting sections are shown in Figure 9; the same model was used in *PDStrip*.

Figure 10 shows a grid on the half ship (973 panels), automatically generated by *GL Rankine*, which was used in *GL Rankine* computations.

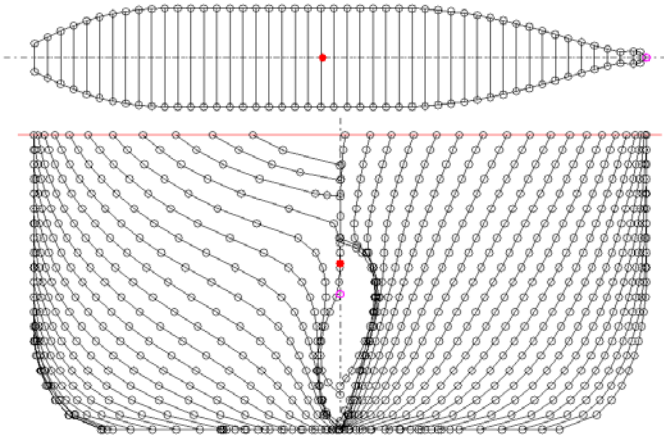

Figure 9: Sectional offsets for Ship D used in *OCTOPUS* and *PDStrip*

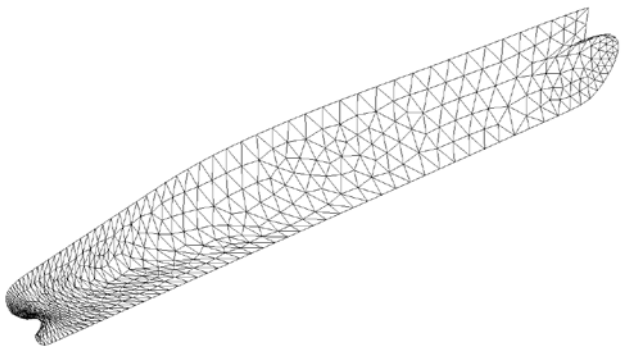

Figure 10: Panel mesh for Ship D used in *GL Rankine* computations

RESULTS

Predictions from all codes are compared with model tests in this section. For Ship F and Ship G, also results from *Vantorre and Journée (2003)* computed with *OCTOPUS* are shown, labelled OCTOPUS 2003. For Ship D, *OCTOPUS* and

AQUA+ results from *Vantorre et al. (2008)* are shown in addition, labelled OCTOPUS 2008 and AQUA+ 2008, respectively. *AQUA+* is a boundary element ship motion code developed by École Centrale de Nantes.

With *GL Rankine* and *WAMIT*, calculations were done using two different methods: "fixed method", when the ship is free to heave, roll and pitch but is fixed at the centre of gravity in surge, sway and yaw, to replicate the model test setup, and "free method", when the ship is free to oscillate in all six degrees of freedom (this is how calculations were done with *AQWA*, *MOSES*, *OCTOPUS* and *PDStrip*), to provide comparison data for the other codes.

Figure 17 shows the wave-induced heave force and pitch moment for each case, calculated using *OCTOPUS.*

Table 4 summarises absolute difference between each method and the experimental results, averaged over all frequencies for which experimental data exist. These differences are in the same units as the RAOs. To calculate the "absolute difference" values for *GL Rankine* and *WAMIT*, the results of the "fixed" method were used. These results are also shown graphically in Fig. 18.

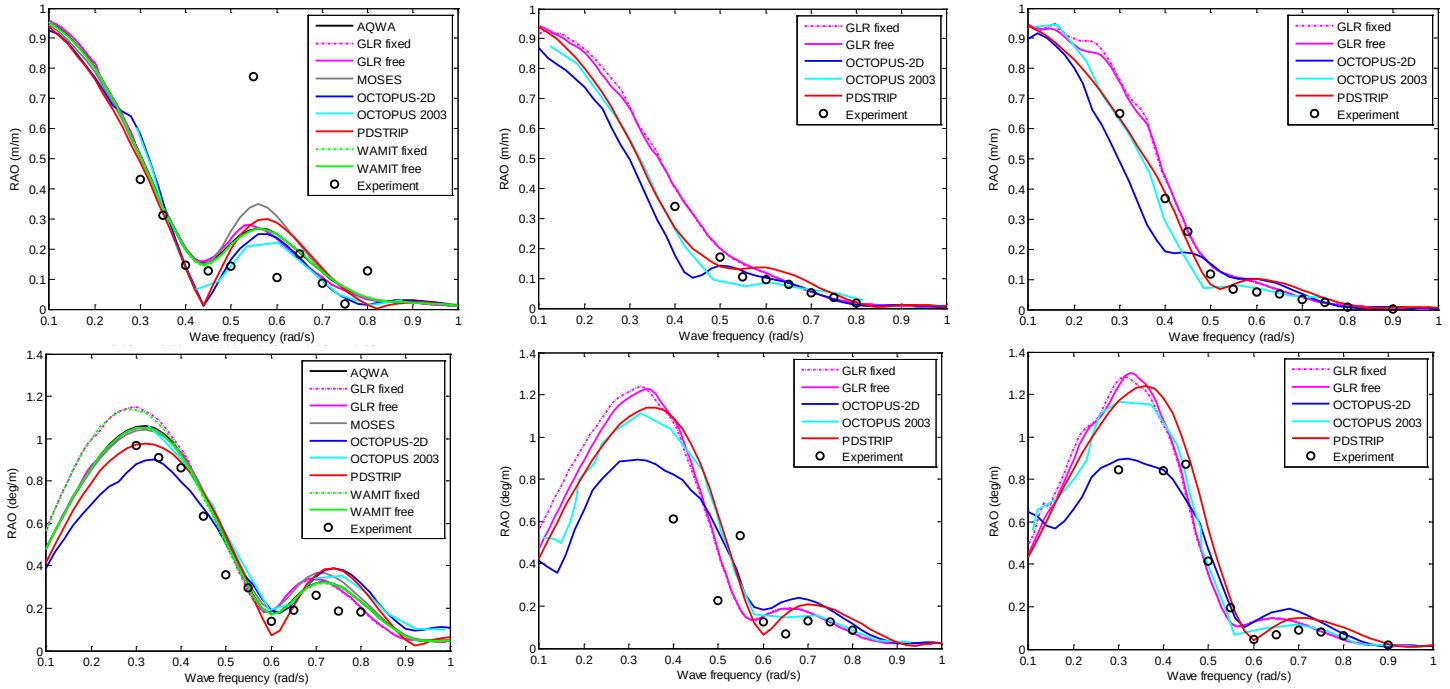

Figure 11: Heave (top) and pitch (bottom) of Ship F in head waves at 0.0 (left), 8.0 (middle) and 12.0 (right) knots

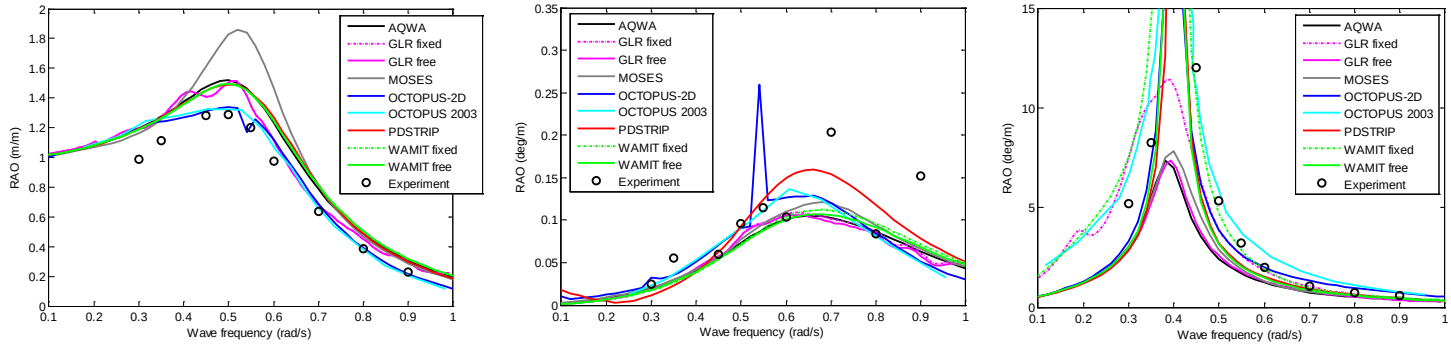

Figure 12: Heave (left), pitch (middle) and roll (right) of Ship F in beam waves at zero forward speed

Figures 11 and 12 show results of computations in comparison with experiments for Ship F: heave and pitch in head waves at the forward speed of 0.0, 8.0 and 12.0 knots, Figure 11, and heave, pitch and roll in beam waves at zero forward speed, Figure 12.

Looking firstly at heave in beam waves, we see that the peak in heave RAO of Ship F is at the wave frequency of about 0.5 rad/s at the considered water depth. The natural heave frequency as calculated in WAMIT is 0.55 rad/s, and the wave-induced heave force has a peak at lower wave frequencies, Fig. 16. Heave in beam waves is predicted well by most codes.

In head waves at zero speed, the heave RAO peaks and troughs generally follow the wave-induced heave force shown in Fig. 17.

However, the model tests showed a large peak at 0.55 rad/s, which corresponds to the heave resonance frequency. The model test time trace at this frequency, Fig. 13, showed a slow build-up of heave amplitude, consistent with resonance. A similarly large heave amplitude was observed in the Ship F model tests at 0.55 rad/s in following waves. This apparent phenomenon of heave resonance in head and following waves at zero speed was checked using other zero-speed cases within the same experimental program. For Ship D at 11.6 m draft at the depth of 14.0 m with waves 10° off-stern, a large heave RAO of 0.75 m/m was measured at a wave frequency of 0.50 rad/s. This frequency corresponded to the natural heave frequency calculated using *WAMIT*, suggesting that heave resonance occurred also in this case.

For Ship F at zero speed, the head-sea resonance heave peak at 0.55 rad/s was significantly under-predicted by all codes. This suggests that heave damping may be over-predicted at the resonance frequency. Further research is required to investigate the behaviour of the ship in these conditions.

For Ship F, pitch in beam waves shows a peak at the wave frequency of about 0.7 rad/s. The natural pitch frequency calculated with *WAMIT* is 0.69 rad/s, and the wave-induced pitch moment remains fairly constant with wave frequency,

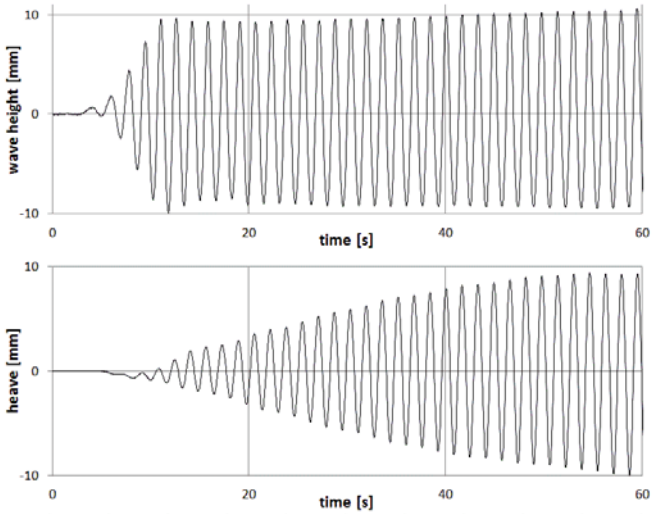

Figure 13: Measured heave motion of Ship F at scale 1:50 in head waves at zero speed, full-scale wave frequency 0.55 rad/s

Fig. 17. In this case, *OCTOPUS* showed erratic results at the wave frequency of 0.54 rad/s, which were traced back to the heave and pitch damping coefficients.

In head waves, the predicted peaks of pitch motion follow in general the wave-induced pitch moment, Fig. 17, which has peaks at the wave frequencies of about 0.30 and 0.75 rad/s.

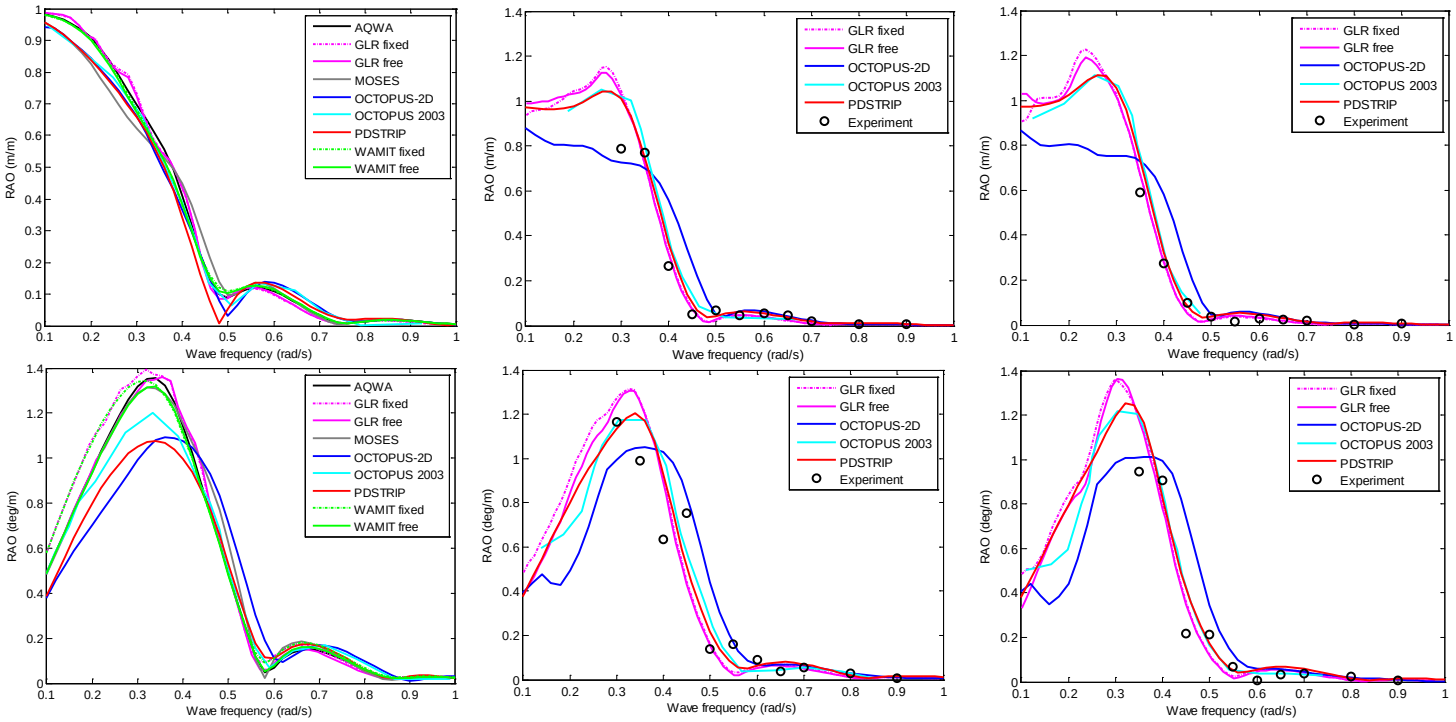

Figure 14: Heave (top) and pitch (bottom) of Ship G in head waves at 0.0 (left), 8.0 (middle) and 10.0 (right) knots

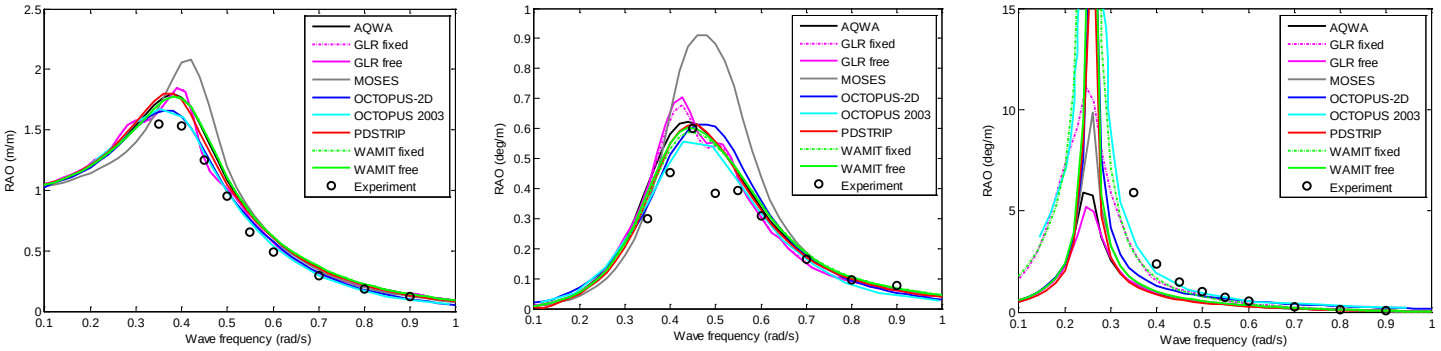

Figure 15: Heave (left), pitch (middle) and roll (right) of Ship G in beam waves at zero forward speed

Results of *GL Rankine* and *WAMIT* in head waves show noticeably larger pitch motions for the "fixed" case, i.e. when the ship is held fixed in surge, compared to the "free" case, when surge is unrestrained. Roll in beam waves indicates that the natural roll frequency is about 0.4 rad/s, and that this natural frequency is predicted well by all codes. As stated above, all codes use different roll damping characteristics, and the authors did not attempt to fit roll damping characteristics between the different codes. Note that the case when the ship is fixed in sway produces noticeably larger roll motions than the case with unrestrained sway, as calculated with *GL Rankine* and *WAMIT*.

Figures 14 and 15 show results of computations for Ship G in comparison with experiments: heave and pitch in head waves at the forward speeds of 0.0, 8.0 and 10.0 knots, Figure 14, and heave, pitch and roll in beam waves at zero forward speed, Figure 15. Note that no model test results were available for heave and pitch in head waves at zero speed.

Heave motions in beam waves indicate a peak at the wave frequency of about 0.40 rad/s. The natural heave frequency calculated with *WAMIT* is 0.42 rad/s, and the wave-induced heave force indicates a peak at lower wave frequencies, Fig. 17. Heave in beam waves is predicted well by most codes. Heave in head waves is also predicted well for the cases with non-zero forward speed. Note the rapid decrease of heave motions with increasing wave frequency for this heavy-displacement ship.

Experimental results of pitch motions in beam waves show a somewhat erratic behaviour around the peak of pitch motions at the wave frequency of about 0.5 rad/s, which indicates the difficulty of predicting pitch near the peak in beam waves. The natural pitch frequency calculated with *WAMIT* is 0.50 rad/s. Nevertheless, the numerical predictions are in general good over the entire wave frequency range.

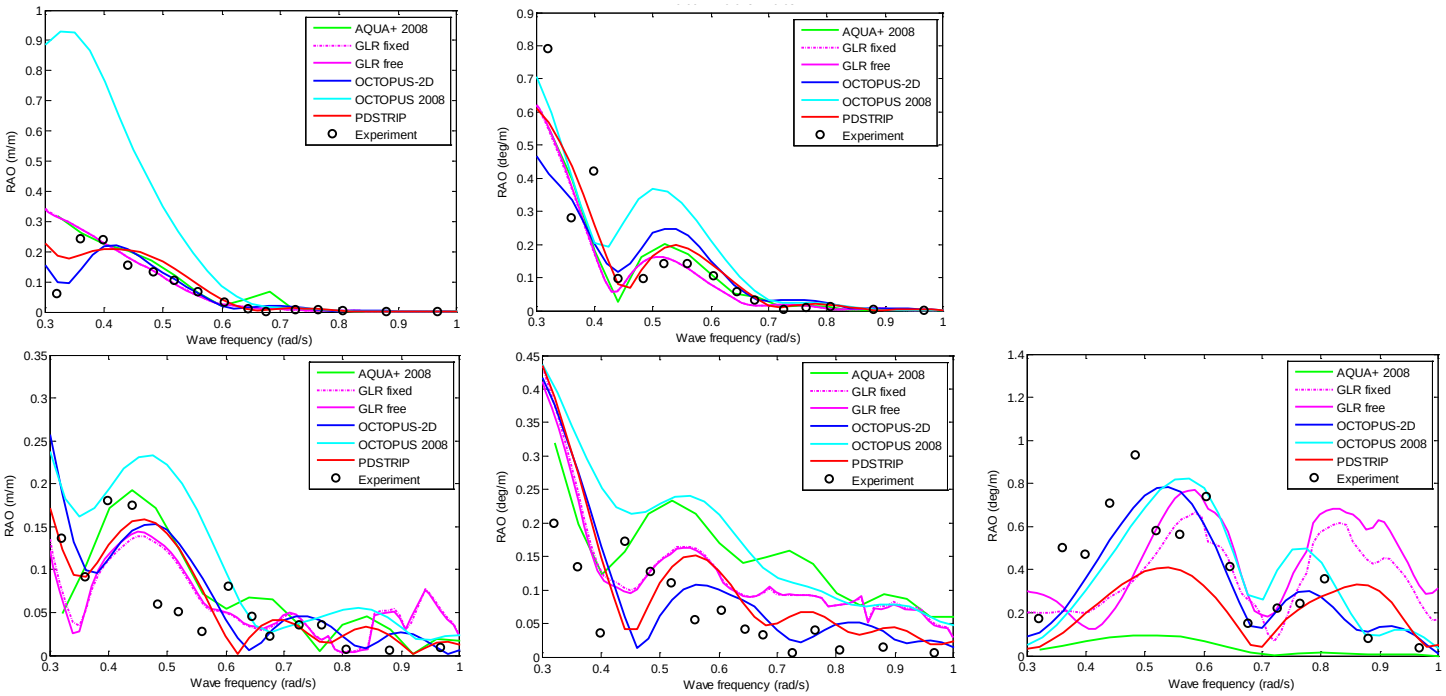

Figure 16: Heave (left), pitch (middle) and roll (right) of Ship D in head waves (top) and in waves 10° off-stern (bottom) at 12.0 knots forward speed

Table 4: Differences between numerical and experimental results

Ship	Wave Direction	Speed [knots]	DOF	*AQWA*	*GL Rankine*	*MOSES*	*OCTOPUS*	*PDStrip*	*WAMIT*
Ship F	head	0.0	heave	0.101	0.099	0.105	0.103	0.103	0.099
Ship F	head	8.0	heave	-	0.021	-	0.030	0.031	-
Ship F	head	12.0	heave	-	0.028	-	0.052	0.024	-
Ship F	head	0.0	Pitch	0.081	0.097	0.096	0.082	0.081	0.084
Ship F	head	8.0	Pitch	-	0.156	-	0.145	0.184	-
Ship F	head	12.0	Pitch	-	0.103	-	0.057	0.103	-
Ship F	beam	0.0	heave	0.180	0.131	0.289	0.071	0.178	0.179
Ship F	beam	0.0	Pitch	0.031	0.030	0.028	0.039	0.029	0.031
Ship F	beam	0.0	Roll	2.110	1.310	1.900	1.140	1.530	1.200
Ship G	head	8.0	heave	-	0.045	-	0.064	0.042	-
Ship G	head	10.0	heave	-	0.020	-	0.070	0.029	-
Ship G	head	8.0	Pitch	-	0.109	-	0.098	0.095	-
Ship G	head	10.0	Pitch	-	0.071	-	0.096	0.072	-
Ship G	beam	0.0	heave	0.131	0.084	0.207	0.059	0.118	0.136
Ship G	beam	0.0	Pitch	0.060	0.056	0.166	0.058	0.049	0.051
Ship G	beam	0.0	Roll	0.890	0.510	0.860	0.700	0.920	0.510
Ship D	head	12.0	heave	-	0.026	-	0.028	0.031	-
Ship D	head	12.0	Pitch	-	0.062	-	0.073	0.057	-
Ship D	10°	12.0	heave	-	0.043	-	0.050	0.039	-
Ship D	10°	12.0	Pitch	-	0.076	-	0.066	0.071	-
Ship D	10°	12.0	Roll	-	0.196	-	0.113	0.214	-

At non-zero forward speed in head waves, pitch motion shows a peak at the wave frequency of about 0.3 rad/s, where the wave-induced pitch moment has a maximum, Fig. 17. Similarly to heave motions, pitch motions of Ship G are very small at higher wave frequencies due to the heavy displacement of this ship. No model test results were available for roll in beam waves near the resonance roll frequency of 0.26 rad/s, thus limited conclusions can be drawn. However, similarly to Ship F, the importance of sway-roll coupling is clearly seen from the comparison of the "fixed" and "free" results.

Figure 16 compares computed heave, pitch and roll of Ship D in head waves and in waves 10° off-stern at the forward speed 12.0 knots with experiments. Heave generally follows the wave-induced heave force, Fig. 17. Reasonable agreement is shown with the experiments for heave at both wave headings. For both wave headings, pitch roughly follows the wave-induced pitch moment. Reasonable agreement is shown between the numerical predictions and experimental results.

For waves 10° off-stern, roll motions essentially follow the wave-induced roll moment. Some of the numerical results show additional dynamic amplification at wave frequencies of 0.8 to 0.9 rad/s, where the encounter frequency comes close to the natural roll frequency of 0.40 rad/s.

CONCLUSIONS

Ship under-keel clearance management in navigation channels and at the berth requires accurate calculation of ship wave-induced motions in shallow water, as well as a thorough understanding of the accuracy and limitations of the methods used. Another application area that requires accurate predictions of seaway-induced ship motions in shallow water is analysis of transport, installation and service operations for offshore wind parks. So far, publications concerning benchmarking of different numerical methods for the prediction of motions in waves in shallow water have not been available in the open literature. This paper aims to make a first step in this direction and provide benchmarking of modern commercially available numerical codes to predict ship motions in waves in shallow water.

The benchmarking showed in general good agreement of numerical predictions with model test results for three cargo ships studied over the entire range of wave frequencies. In addition, results at non-zero forward ship speed demonstrated similar accuracy to the results at zero forward speed.

The codes showed no particular trend to over-predict or under-predict the wave-induced motions, with the model test results generally deviating both above and below the numerical predictions for each code. Therefore, we may expect that when combining transfer functions of ship motions with energy spectra of irregular seaways, motion response spectra and spectral characteristics of ship motions in irregular waves may be reasonably well predicted.

It must be borne in mind that, due to the limited width of available towing tanks, suitable for accurate measurements of ship motions in shallow water, the presented results consider a limited range of ship speed and wave direction combinations. Further benchmarking for various ships at different forward speeds in bow-quartering, beam, stern-quartering and following waves is desirable, using tests with self-propelled models in a wave basin.

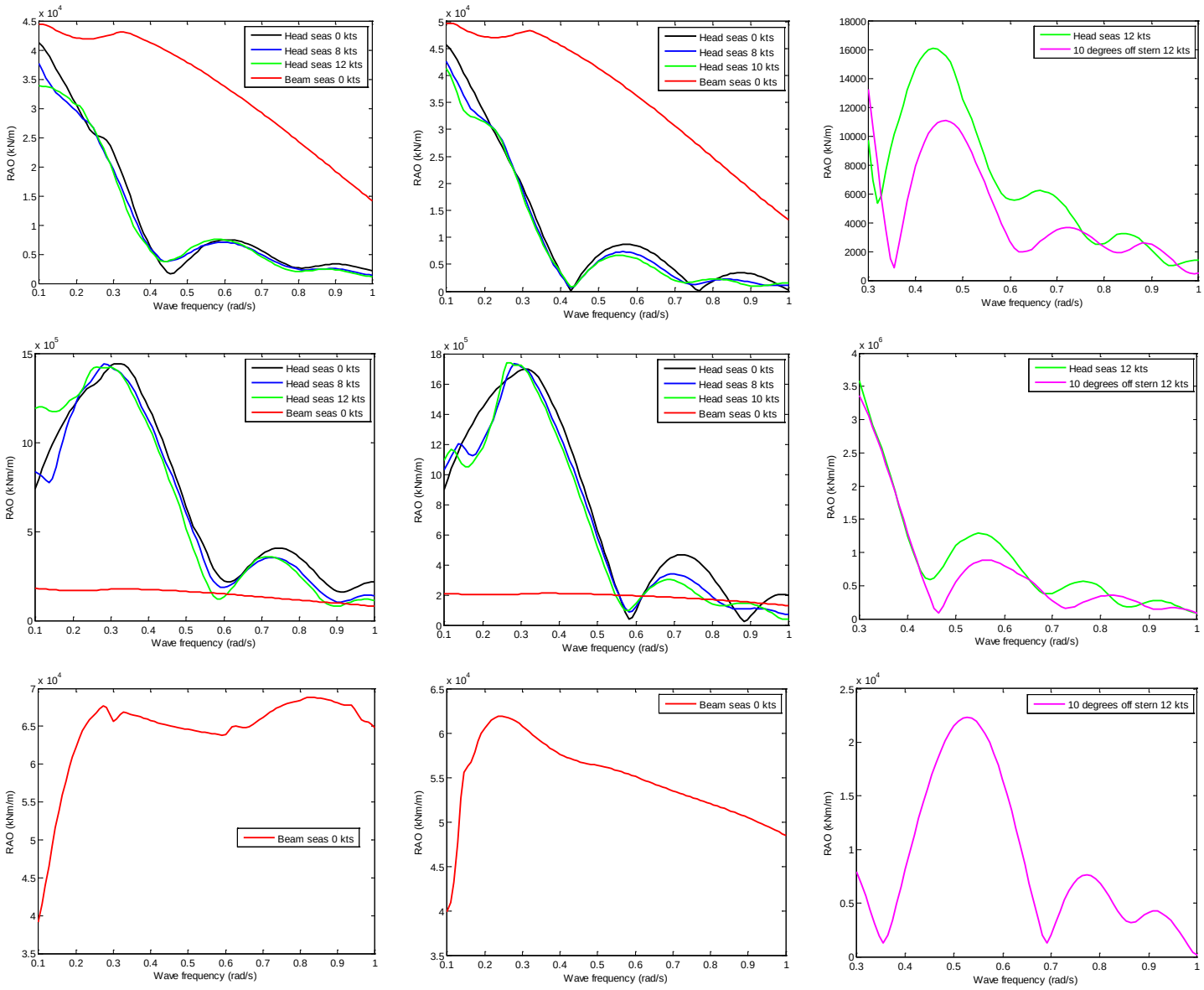

Figure 17: Wave-induced heave force (top), pitch moment (middle) and roll moment (bottom) of Ship F (left), Ship G (middle) and Ship D (right) calculated with OCTOPUS

ACKNOWLEDGEMENTS

The authors are thankful for the cooperation of Flanders Hydraulics Research and Ghent University in providing ship and model test data for this benchmarking study. We also acknowledge the assistance of Amarcon, Bentley Systems, Professor H. Söding and WAMIT Inc. in checking input and output for their respective codes. Mr. A. Köhlmoos, DNVGL SE Hamburg, is acknowledged for performing numerical computations with *AQWA* software.

REFERENCES

[1] Amarcon (2009) *Octopus-Office 6 User Manual*, July 2009

[2] Ansys Inc. (2010) *ANSYS AQWA Users Manual*

[3] von Graefe, A. (2014) Rankine source method for seakeeping analysis in shallow water. *Proc. ASME 33rd Int. Conf. on Offshore Mechanics and Arctic Eng. OMAE 2014*, San Francisco, USA

[4] Journée, J. M. J. (2001) *Verification and Validation of Ship Motions Program SEAWAY.* Techn. Rep. 1213a, Ship Hydromechanics Laboratory, Delft University of Technology

[5] Journée, J. M. J., and Adegeest, L. J. M. (2003) *Theoretical Manual of Strip Theory Program "SEAWAY for Windows"*. Rep. Nr. 1370, Ship Hydromechanics Laboratory, Delft University of Technology

[6] Söding, H. (2006) *Program PDSTRIP: Public Domain Strip Method.* Retrieved from www.sourceforge.net

[7] Söding, H., von Graefe, A., el Moctar, O. and Shigunov, V. (2012) Rankine source method for seakeeping predictions, *Proc. 31st Int. Conf. on Ocean, Offshore and Arctic Eng. OMAE2012*, Rio de Janeiro, Brasil
[8] Ultramarine Inc. (2012) *Reference manual for MOSES*
[9] Vantorre, M., Laforce, E., Eloot, K., Richter, J., Verwilligen, J., and Lataire, E. (2008) Ship motions in shallow water as the base for a probabilistic approach policy. *Proc. ASME 27th Int. Conf. on Offshore Mechanics and Arctic Engineering OMAE 2008*, Estoril, Portugal
[10] Vantorre, M., and Journée, J. M. J (2003) Validation of the strip theory code SEAWAY by model tests in very shallow water. *Numerical Modelling Colloquium*, Flanders Hydraulics Research, Antwerp, October 2003. DUT-SHL Report Nr. 1373-E
[11] Vantorre, M., Verzhbitskaya, E., and Laforce, E. (2002) Model test based formulations of ship-ship interaction forces, *Ship Technology Research* **49**(3) 124-141
[12] WAMIT Inc. (2013) *WAMIT v7.062 User Manual*
[13] Keil, H. (1974) *Die Hydrodynamische Kräfte bei der periodischen Bewegung zweidimensionaler Körper an der Oberfläche flacher Gewasser* (in German), Rep. Nr. 305, Institut für Schiffbau, University Hamburg

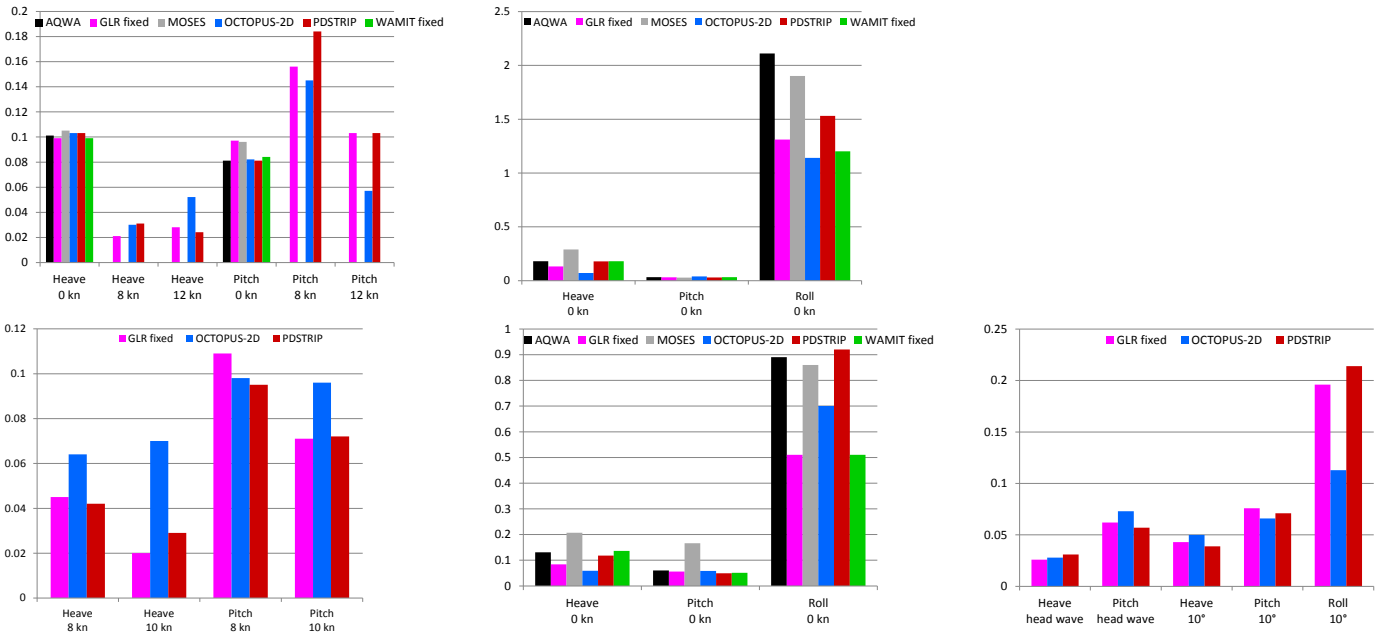

Figure 18: Differences between numerical and experimental results according to Table 4. Top left: Ship F, head waves; top middle: Ship F, beam waves; bottom left: Ship G, head waves; bottom middle: Ship G, beam waves; bottom right: Ship D